Effect of addition of aluminum phosphinate as fire retardant in a PBT vitrimer

Louis Meunier, Damien Montarnal, David Fournier, Valérie Gaucher, Sophie Duquesne, Fabienne Samyn

Effect of addition of aluminum phosphinate as fire retardant in a PBT vitrimer

Louis Meunier[1], Damien Montarnal[2], David Fournier[1], Valérie Gaucher[1], Sophie Duquesne[1], Fabienne Samyn [1*]

[1] Univ. Lille, CNRS, INRAE, Centrale Lille, UMR 8207 - UMET - Unité Matériaux et Transformations, F-59000 Lille, France,

[2] Univ. Lyon, Université Claude Bernard Lyon 1, CPE Lyon, CNRS, UMR 5265, Chemistry, Catalysis, Polymers and Processes, F-69616 Villeurbanne, France

Corresponding author:

*fabienne.samyn@centralelille.fr,

ENSCL@Centrale Lille Institut, Bat. C7, avenue Mendeleïev, Cité Scientifique, 59650 Villeneuve d'Ascq, France

Abstract

This work investigates the effect of flame-retardant additives on the thermo-mechanical and dynamic properties of poly(butylene terephthalate) (PBT) vitrimers. The vitrimers were synthesized and compounded in a single step by reactive extrusion from commercially available PBT, an epoxy resin, a zinc-based transesterification catalyst, and aluminum phosphinate (AlPi) as a conventional flame retardant additive. We demonstrated that the presence of AlPi in relatively large amount (20 wt.-%) is compatible with the formation of the vitrimer network and does even play the role of a transesterification (co)catalyst accelerating the exchange reactions and improving the processability of the vitrimer. UL-94 flammability tests also confirm the effective role of AlPi as flame retardant in vitrimer.

Key words: Vitrimer, reactive extrusion, PBT, flame retardancy, phosphinate

I. INTRODUCTION

Poly(butylene terephthalate) is a semi-crystalline thermoplastic polyester commonly used for electrical and electrotechnical applications (E&E).[**1**] This polymer has several drawbacks. Firstly, its chains are barely entangled due to both a high critical entanglement molecular weight (M_c about 60 $kg.mol^{-1}$) [**2**] and the difficulty to synthesize PBT with very high molecular weight.[**3–7**] Consequently, around the melting point, the low viscosity of the unfilled polymer may induce a loss of the dimensional stability of PBT materials [**7**] as well as dripping. In addition, this polymer is flammable. The commercial grades PBT employed for E&E parts production are consequently generally

formulated with specific additives such glass fibres and flame-retardants to reach acceptable level of mechanical and fire performances.

Converting a thermoplastic polymer into a vitrimer is an approach actually under investigation by academics to improve their performances. The term vitrimer describes a new class of polymers introduced in 2011 by Leibler *et al.* [**8**]. This family consists in dynamic, covalently cross-linked polymer networks having interesting properties thanks to the exchangeable links present in their structure. Under a thermal stimulation, associative bond exchange reactions are triggered enabling topology rearrangement leading to polymer malleability without decrease of the cross-linking density. Self-healing, recyclability and improved mechanical performances are common features of vitrimers.[**9**] During the last decade, numerous bond exchange reactions potentially applicable to vitrimers have been reported, such as transesterification [**8**], imine [**10, 11**], olefin [**12, 13**] and dioxaborolane [**14, 15**] metathesis, transalkylation of triazonium salts [**16**], transesterification of boronic esters [**15**] and phosphate triesters [**17**], and amine exchange of vinylogous urethane.[**18–24**] These dynamic networks can be synthesized from thermoplastic precursors in presence of a crosslinker by reactive processing such as reactive extrusion [**25, 14, 26–29**].

Demongeot *et al.* were the first to report the preparation of a PBT vitrimer using reactive extrusion. [8] They introduced dynamic ester-based cross-links using epoxy as chain extender and crosslinker in presence of a transesterification catalyst. Zhou *et al.* then studied the formation of PBT vitrimers via solid state polymerization using glycerol derivatives in presence of a Zn based catalyst.[**30, 31, 32**] In both studies, semi-crystalline vitrimers were obtained. A small drop in the crystallinity was observed compared to PBT. Transesterification reactions in these materials enable to reprocess to a certain extent the materials while maintaining excellent dimensional stability thanks to the cross-linked network.[**25–32**] Farge *et al.* more recently studied the rheological properties as well as the development of plasticity in PBT/epoxy based vitrimers. They showed that those materials exhibited better mechanical performances than PBT as they did not exhibit a strain localization but a stronger strain hardening phenomenon.[**33, 34**]

If many studies are focused on the synthesis and characterization of various properties of vitrimer matrices, their formulation for the final applications has barely been studied and particularly in the field of fire resistance. Reactive or additive approaches are used to impart flame retardancy to a polymer. The reactive pathway consists in modifying the polymer main or side chains in order to incorporate chemical moieties on it (halogenated or phosphorus groups as examples) while the additive approach consists in dispersing flame-retardant additives in the matrix (no covalent link between both phases). In the few studies dedicated to fire retardancy of vitrimers, precursors with intrinsic flame retardancy have been used (reactive approach), such as cyclotriphosphazene-linked

epoxy resin cured with disulfide-containing aromatic diamine [**35**], phosphonate-based vitrimer [**36**] or phosphate ester-based vitrimers.[**37, 38**] Flame retardant additives in conventional vitrimer formulations have however been completely overlooked to date, even though such additives are widely present in commercial thermoplastics.

On the other hand, efficient flame-retardant additives for PBT are mainly composed of phosphorus-containing compounds, like phosphine oxides [**39**], aromatic phosphates [**40-42**], phosphonates [**43-45**], phosphinate salts [**46-48**], or phosphorus-nitrogen [**49**] compounds, sometimes combined with synergists acting in the solid phase to offset the low-charring nature of PBT.[**42, 45, 46, 47**] These additives are added at loading from 10 up to 60 wt.-%.

According to this literature review, the question arises whether incorporation in such amounts of additives impacts the dynamics of the exchange reactions. The incorporation of additives in vitrimer matrices remains marginally studied and limited to the use of nanoparticles such as silica [**50**] (up to 40 wt.-%), graphene [**51,52**] (up to 1wt.-%), cellulose [**53**] (up to 15 wt.-%) or carbon nanotubes [**54**] (up to 3 wt.-%). These studies nevertheless evidence that their presence could influence the dynamics of exchange reactions either increasing [**50**] or decreasing [**53**] the relaxation time.

This work consequently aims at investigating the possibility to fireproof a PBT vitrimer via the incorporation of a flame-retardant additive. Vitrimers were synthesized by reactive extrusion from a commercially available PBT, an epoxy resin and a zinc-based transesterification catalyst. Aluminum phosphinate was selected as flame-retardant additive as it is known for its efficiency to flame retard PBT without the addition of synergist. The impact of the use of this flame retardant (FR) on the exchange reactions as well as on the thermal, mechanical and fire properties of the new materials was evaluated. In the first part of this paper, formulations with the strict addition of aluminum phosphinate were studied, while in the second part, catalyst-free formulations were analyzed to further investigate the role played by the flame-retardant on the matrix behavior.

II. Experimental section

2.1. Materials

PBT was obtained from SABIC under the name Valox 315, with an end-group concentration [COOH] = 37 mEq/kg and [OH] = 120 mEq/kg and Mn = 47000 g/mol. Bisphenol A diglycidyl ether (DGEBA; >96%) and Zinc(II) acetylacetonate hydrate ($Zn(acac)_2$, xH_2O ; >99%) were purchased from Sigma-Aldrich. Aluminum diethylphosphinate (AlPi, Exolit OP 1230, average particle size from 20 to 40 µm) was purchased from Clariant. 1,1,1,3,3,3-

hexafluoroisopropanol (HFIP ; >99%) was purchased from Fluorochem. The chemical formulas of the different raw materials are given in **Figure 1**.

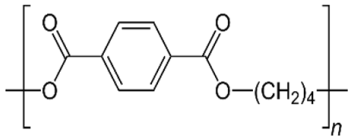

Poly(butylene terephtalate), PBT

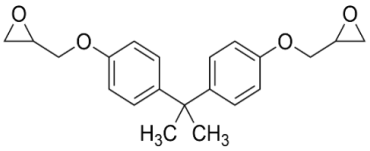

Epoxy resin, DGEBA

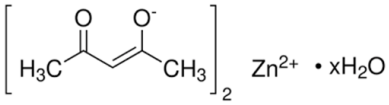

Zinc acetylacetonate hydrate, $Zn(acac)_2$, xH_2O

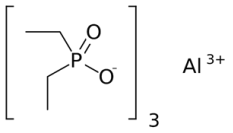

Aluminum diethylphosphinate, AlPi

Figure 1. Chemical structures of the chemicals used in this study

2.2. Processing

The formulations and work-up is based on the study of Demongeot et al. [**25**] Formulations from **Table 1** were prepared using a twin-screw extruder (15 cm^3 DSM micro-explorer) under nitrogen flux to prevent oxidation. Poly(butylene terephthalate) and aluminum diethylphosphinate were dried at 80°C overnight before processing. The molar ratios used in this study were fixed at 2:1 for [epoxy]/([OH]+[COOH]) and 0.11:1 for [catalyst]/([OH]+[COOH]). Aluminum phosphinate was incorporated at 20 wt.-%, which is a typical loading used to achieve the flame-retardant performances with this additive. The total volume of reactants was fixed at 10 cm^3 to keep the torque below 7000 N. The different components of the formulations were premixed before their introduction in the extruder and then processed at 270°C and 60 rpm. The torque, which is indicative of the viscosity of the material, was recorded as a function of the residence time during each test. After 8 minutes, the obtained formulation was extracted from the extruder. To shorten the materials names, the following abbreviations will be used: E for epoxy, Z for the transesterification catalyst and A for the aluminum phosphinate. As an example, the material referred to as PBT-EZA was formulated with PBT, epoxy resin, zinc acetylacetonate and aluminum phosphinate. In this study, the focus is on the potential reactivity of flame retardant fillers with the vitrimer matrix. No antioxidant was added in our formulations considering that the addition of antioxidants, as done in other researches [**25, 33, 34**], could impact this reactivity and that interactions between antioxidant and flame retardant could also happen.

Table 1. Summary of the prepared formulations.

Sample	Mass of components (g)			
	PBT	DGEBA (E)	$Zn(acac)_2$ (Z)	AlPi (A)
PBT	12	/	/	/
PBT-A	9.7	/	/	2.41 (20 wt.-%)
PBT-EZ	11.7	0.23 (1.9 wt.-%)	0.021 (0.18 wt.-%)	/
PBT-EZA	9.5	0.19 (1.6 wt.-%)	0.017 (0.14 wt.-%)	2.41 (20 wt.-%)
PBT-EA	9.5	0.19 (1.6 wt.-%)	/	2.41 (20 wt.-%)

Specimens for the fire, rheology and mechanical tests were prepared using a DSM Xplore 12 cm^3 Laboratory Injection-Molding Machine. The injection temperature was set to 270°C and the mold temperature to 100°C.

2.3. Characterization methods

Elemental analysis. The mass contents of Al and P in the formulations were determined using ICP-AES (iCAP 6500 Duo, Thermo Scientific). Samples were cryoground and mineralized in an acidic environment before their analysis. The fraction of AlPi in the material (FR_m) was calculated by considering only the amount of phosphorus inside the material ($\%P_m$), using the **Equation 1**. $\%P_{FR}$, the weight percentage of phosphorus in AlPi is equal to 24%, according to supplier. This formula will be used to calculate the FR fraction of the formulation or its gel part. For the soluble part, the calculation is detailed in the supporting informations.

Equation 1

$$\%\boldsymbol{FR_m} = \mathbf{100} \times \left(\frac{\%\boldsymbol{P_m}}{\%\boldsymbol{P_{FR}}}\right)$$

Gel and soluble fraction separation. 200 mg of each formulation (m_0) were immersed in 20 mL of HFIP, a well-known solvent for Poly(butylene terephthalate) [**32, 55**] that is also a solvent for AlPi, for 4 days under stirring at room temperature and filtered using a Büchner funnel. The insoluble gel fraction collected on the filter was dried for 4 days at room temperature and then weighed (m_{gel}).

The gel ratio for the materials without FR can be directly calculated as the mass of the insoluble part divided by the initial mass of the sample.

For the flame retarded materials, the gel ratio can be calculated including or excluding the amount of flame retardant. In the case the FR is included, a global gel ratio ($\%Gel_{PBT+FR}$) is calculated using **Equation 2.1** and when the FR part is excluded, the gel ratio was calculated using **Equation 2.2**

Equation 2 $$\mathbf{1}.\ \%\mathrm{Gel}_{\,PBT+FR} = 100 \times \frac{\boldsymbol{m_{gel}}}{\boldsymbol{m_0}}; \quad \mathbf{2}.\ \%\mathrm{Gel}_{\,PBT} = 100\times\frac{\boldsymbol{m_{gel}\,(100-\%FR_{gel})}}{\boldsymbol{m_0\times(100-\%FR_0)}}$$

with m_o and $\%FR_0$ respectively the initial mass and the FR fraction contained in the formulation and m_{gel} and $\%FR_{gel}$ respectively the weight of gel and the FR fraction contained in the gel part of the formulation.

The global gel ratio value will be considered when discussions about the formulation properties will be performed (flow and mechanical sections) and in the section dealing with the effect of adding FR on the crosslinking of the matrix, the gel ratio value without the FR part will be considered.

In parallel, the filtrate was evaporated to recover the solubilized fraction. The vitrimer soluble part and gel fractions are referred to in the following using either a “sol” or “gel” subscript (PBT-EA_{sol} or PBT-EA_{gel} for instance).

SEM microscopy and EPMA. The work was carried out on the Electron microscopy facility of the Advanced Characterization Platform of the Chevreul Institute. The morphology of the materials was characterized by scanning electron microscopy (SEM) using a Jeol JSM-IC 848 SEM with an acceleration voltage of 15 kV. A Cameca SX100 electron probe microanalyzer (EPMA) was used to perform elemental analysis. X-ray mappings were carried out at 15 kV and 40 nA. A TAP crystal is used to detect the Al K_α X-ray and a PET crystal to detect the P K_α X-ray. The samples were embedded into epoxy resin, polished with SiC polishing sheets from grade 80 up to grade 4000 and carbon coated with a Bal-Tec SCD005 sputter coater.

Solid-state NMR analysis. Solid-state (ss) NMR has been used to follow the environment changes of the phosphorus and aluminum nuclei in the formulations. The analyses were carried out on the NMR facility of the Advanced Characterization Platform of the Chevreul Institute using a Bruker Avance II 400 on cryoground samples.

^{31}P ss NMR measurements were performed at 40.5 MHz using a 4 mm probe, with dipolar decoupling (DD) and magic angle spinning (MAS) at a speed of 20 kHz. The delay time between two impulsions was fixed at 120 s (because of the relaxation time of the phosphorus nucleus). The spectra were acquired after 16 to 32 scans to get a correct signal-to-noise ratio. The reference used was 85 % H_3PO_4 in aqueous solution

^{27}Al ss NMR measurements were performed at 104 MHz using a 4 mm probe, with MAS at a speed of 20 kHz. The delay time between two impulsions was fixed at 1 s (quick relaxation time of quadripolar nuclei). 512 to 2048 scans have been acquired to increase the signal/noise ratio. The reference used is a 1 M solution of aluminum nitrate.

Thermal analyses. Differential scanning calorimetry (DSC) analyses were performed using a Discovery DSC from TA Instruments under nitrogen (50 mL/min). Temperature and heat flow were calibrated with a high purity indium sample using standard procedures. The sample (5 mg) was heated in an aluminum pan from -40 to 270 °C at 20 °C/min, held at 270 °C for 2 min, then cooled to -40 °C at 20 °C/min, held at -40 °C for 2 min, and finally heated to 270 °C at 20 °C/min. The crystallinity ratio (χc) was obtained using **Equation 3.1 and 3.2** with $\Delta H_{m100\%}$ the enthalpy of melting for a 100% crystalline PBT (142 J/g) [**56**], ΔH_m the experimentally measured melting enthalpy and $\%FR_m$ the weight percentage of FR in the material. The **Equation 3.1** considers the global crystallinity ratio of the formulation including the FR (AlPi is not crystalline) whereas **Equation 3.2.** excludes the FR fraction from the calculation.

Equation 3.1

$$\chi_{c\ PBT+FR} = \frac{100 \times \Delta H_m}{\Delta H_{m100\%}}$$

Equation 3.2

$$\chi_{c\ PBT} = \frac{100 \times \Delta H_m}{\Delta H_{m100\%} \times (1 - \%\mathrm{FR}_m/100)}$$

Thermogravimetric analyses (TGA) were performed in alumina pans with a gold foil (to prevent reactions between the sample and the crucible) using a Discovery apparatus from TA Instrument under nitrogen flow (20 mL/min). A purge of 60 min at 40 °C was carried out before heating the sample (around 10 mg, powder) from 40 to 800°C at a heating rate of 20°C/min.

Stress relaxation experiments. Stress-relaxation experiments were conducted to record the time and temperature-dependent dynamics of the different PBT vitrimer formulations using an Anton Paar MCR 301 Rheometer equipped with 25 mm diameter plate-plate geometries. Shear strains of 1 % were applied, well within the linear viscoelastic regime of the material, while the gap was maintained at 1.5 mm during the whole experiment. Considering that stress relaxation of vitrimers cannot be described by a single relaxation time (as for polymers), the experimental stress relaxation curves G(t) were fitted using the Kohlrausch-William-Watts (KWW) model of stretched exponentials decay (**Equation 4**).[**57 – 59**]

Equation 4

$$\boldsymbol{G(t) = G_0 e^{-\left(\frac{t}{\tau^*}\right)^{\beta}}}$$

The corresponding initial relaxation modulus G_0 and characteristic relaxation times τ*, were obtained for each temperature by fitting the experimental data with **Equation 4** and applying the same stretching exponent β (0<β<1) to all curves in each serie. This β parameter is related to the breath of distribution of relaxation times (that become monodispersed for β=1). The average relaxation time < τ > was calculated using **Equation 5**, where $\boldsymbol{\Gamma}$ is the gamma function, i.e. $\boldsymbol{\Gamma(x) = \int_0^{+\infty} t^{x-1} e^{-t} dt}$.

Equation 5

$$< \tau >= \boldsymbol{\tau^*} * \frac{\boldsymbol{\Gamma\left(1/\beta\right)}}{\boldsymbol{\beta}}$$

By plotting ln(<τ>) =f(1000/T), it is then possible to verify if the relaxation times vary following an Arrhenius law, which is typical of dynamic networks where chemical exchanges control the viscosity.

Fire test. UL-94 tests were performed in vertical orientation on 125 mm × 12 mm × 3 mm rectangular samples, following the procedure defining the standard IEC 60695-11-10. For each formulation, a set of 5 samples is tested. Each specimen is successively fixed vertically on a testing holder above cotton (distance sample-cotton of 30 ± 0.5 cm). A 20 mm high blue calibrated Bunsen burner flame is applied to the free end of the specimen for 10 s and then removed. The time of burning is recorded (t_1). If the sample extinguished before the clamp, the burner is applied a second time and the flaming time is measured again (t_2). Otherwise the sample is not classified. Depending of the flaming time at each inflammation, the total flaming time of the 5 samples set and the dripping behavior, the sample obtain a specific rating V0, V1 or V2. The best rating is V0 and it is obtained if each sample has $t_1 \leq 10$ s, $t_2 \leq 10$ s, $\boldsymbol{\sum_{i=1}^{5}(t_1 + t_2)_i} \leq 50$ s and there is no flaming dripping. In addition to the rating, each sample was weighted before and after the test in order to evaluate the mass loss during the test.

Mechanical testing. Uniaxial tensile tests were performed using an INSTRON 4466 apparatus equipped with a temperature-controlled chamber regulated at ±1°C. Injected ISO-527-2 dogbone-shaped samples with 35 mm gauge length and 1.5 mm thickness were uniaxially drawn at a constant crosshead speed of 1 mm/min ((i.e. an initial strain rate of ~ 5. 10^{-4} s^{-1}) at 20°C and 160°C.

III. RESULTS AND DISCUSSION

3.1. Reactive extrusion of flame retarded formulation with PBT, Epoxy, $Zn(acac)_2$ and AlPi

The effect of the flame-retardant on the formation of the vitrimer material through reactive extrusion was first studied. The FR materials were synthesized by mixing simultaneously PBT, epoxy, Zn catalyst and AlPi components. **Figure 2** presents the evolution of the torque versus time for this material and reference formulations.

For the reference formulations PBT and PBT-A, the curves show a first rise corresponding to the introduction of the raw materials in the first minutes of processing. Then the torque stabilizes at a lower value (around 500 N) after the melting of the polymer and the dispersion of the additive. No cross-linking nor significant degradation occurs in these cases. For PBT-EZ, on the contrary, a steep rise in axial force is observed after 3 min of residence time reaching approximately 6000 N after 6-7 min. This rise is attributed to an increase in the viscosity due to the reactions between PBT and epoxy in the presence of the Zn(II) transesterification catalyst.[**60**] The same rise is observed when 20 wt.-% aluminum phosphinate is added to the formulation (PBT-EZA). A slightly lower plateau value is achieved (i.e. 4700 N) and a significant acceleration of the cross-linking reactions is observed (torque increase from 90 s). In all cases, the axial force slowly decreases after the maximum force is reached, which may be linked with the occurrence of chain breaks.

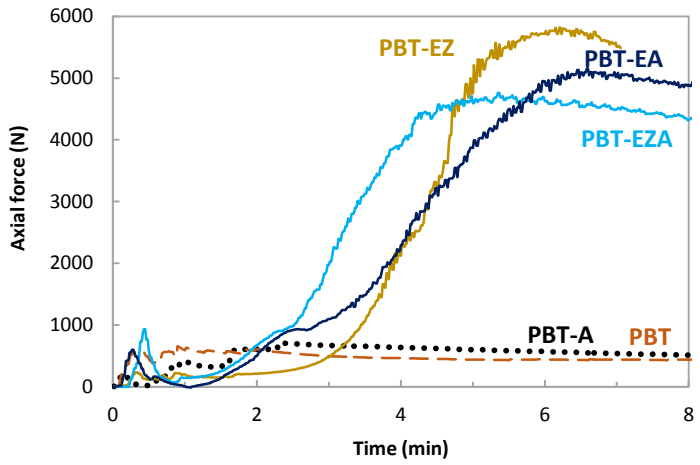

Figure 2. Evolution of the torque recorded during reactive extrusion for PBT, PBT-A, PBT-EZ, PBT-EZA and PBT-EA formulations

To confirm and quantify the formation of cross-linked networks, the gel content of each formulation was determined in HFIP which is at the same time a solvent of PBT and AlPi. While PBT and PBT-A samples are fully soluble as expected, PBT-EZ and PBT-EZA materials present a gel fraction characteristic of a cross-linked network. For PBT-EZ, a gel fraction of 68 (± 4) wt.-% was calculated directly by weighing the insoluble part. For PBT-EZA, a global gel

ratio of 63wt.-% was obtained using **equation 2.1**. The latter includes the part of FR that has not been solubilized. A second gel fraction was also calculated excluding the FR part using **Equation 2.2**. It is representative of the crosslinking of the matrix. To determine it, elemental analysis was performed to quantify the phosphorus content in the formulation and in the gel, then the $\%FR_m$ was calculated using **Equation 1** (**Table 2**). The analyses show that PBT-EZA contains 18.3wt.-% of FR and the gel fraction 11.3 wt% of AlPi. A resulting gel fraction of 69 wt.-% was calculated for PBT-EZA. The global gel ratio is a little bit lower than the gel ratio of PBT-EZ. However, the gel ratio of the matrix fraction ($\%Gel_{PBT}$) is similar to what was obtained for PBT- EZ (68 ± 4 wt.-%) showing that the presence of flame retardant does not prevent the crosslinking to occur.

Table 2. Weight percentages of Aluminum and Phosphorus remaining in PBT-EZA and $PBT\text{-}EZA_{gel}$ based on elemental analysis and calculated $\%FR_m$ and gel ratios

Sample	$\%Gel_{PBT+FR}$	Al (wt.%)	P (wt.%)	$\%FR_m$	$\%Gel_{PBT}$
PBT-EZA	63 ± 3	1.20 ± 0.04	4.35 ± 0.02	18.3	69 ± 3
$PBT\text{-}EZA_{gel}$	/	0.78 ± 0.01	2.70 ± 0.40	11.3	/

Stress-relaxation experiments have been performed on PBT-EZ and PBT-EZA to evaluate the dynamics of the network relaxation at different temperatures. The curves are presented in **Figure 3 - 1** and **Figure 3 - 2**. The presence of a significant fraction of non-cross-linked chains (around 30%) in the dynamic system leads to a complex relaxation behavior. Non-elastically active chains typically lead to fast relaxations (before 1 s), while network relaxations due to bond exchanges occur at longer times (after 10 s). At intermediate times, the presence of a clear plateau characteristic of the cross-linking density is not always observed. Only the second part of the relaxation curve was thus fitted with a Kohlrausch-William-Watts model to estimate the network modulus and relaxation time (See details in **Table S 1** and **Table S 2** in the ESI†).

At comparable temperatures, PBT-EZA exhibits much faster network relaxations than PBT-EZ (by a factor of ca. 100) thus showing that AlPi is considerably active as transesterification catalyst. The temperature-dependence of the network relaxation times for PBT-EZ and PBT-EZA displays an Arrhenius behavior in both cases, with activation energies of 130 and 155 $kJ.mol^{-1}$, respectively, in line with previously reported data on PBT vitrimers (**Figure 3** - 4). [**25, 30**]

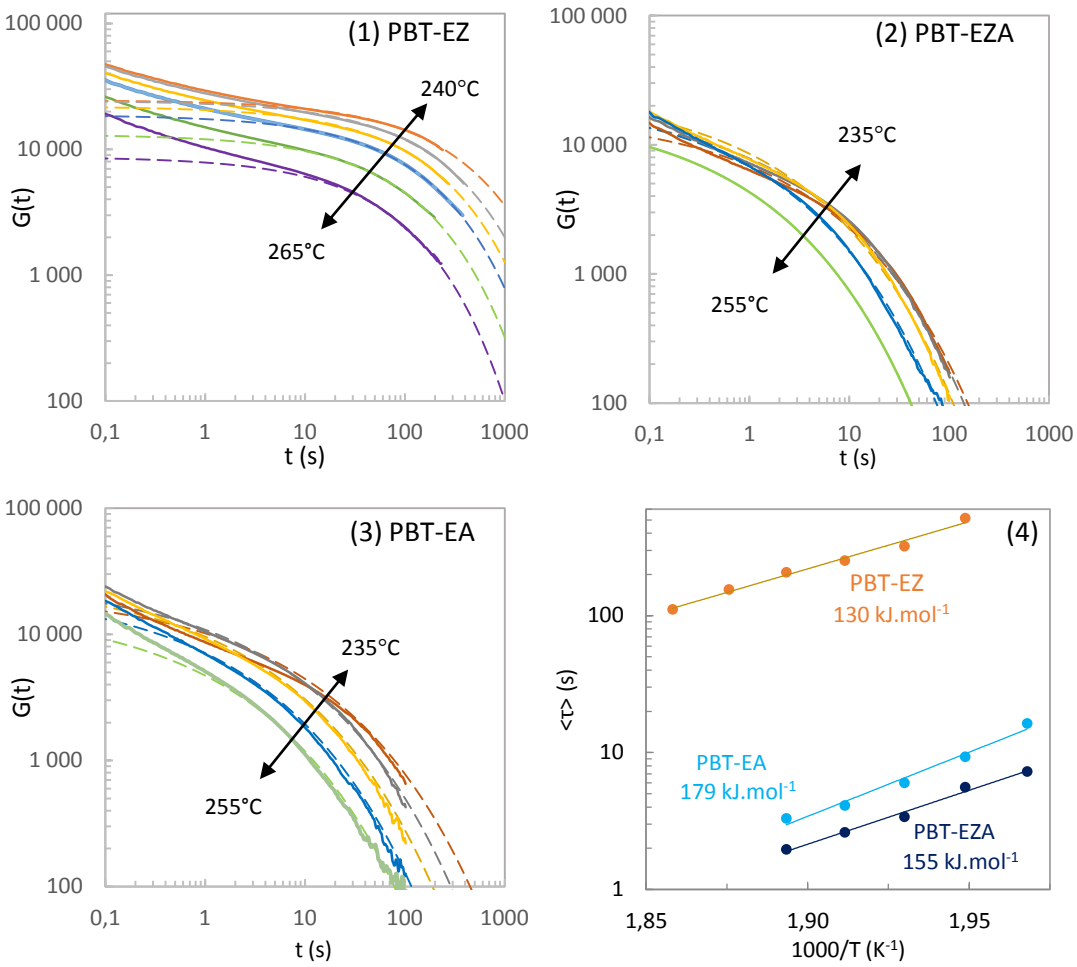

Figure 3. Stress relaxation curves for (1) PBT-EZ, (2) PBT-EZA and PBT-EA (3) at different temperatures. Experimental data in plain line, Kohlrausch-William-Watts model in dotted line, (4) Arrhenius plots of the network relaxation times.

Thermal properties of the materials are reported in **Table 3** and thermograms presented in **Figure S 2**. In addition to the previously studied formulations, the thermal characteristics of the gel and soluble part of PBT-EZ and PBT-EZA were also analyzed.

The vitrimer samples, PBT-EZ and PBT-EZA, have similar glass transition temperatures (T_g around 47°C), which is significantly higher compared to PBT and PBT-A (T_g around 40°C) due to cross-linking leading to a decrease in the mobility of the network. This difference is also observed between the gel (T_g around 47°C) and solubilized fractions of the materials (T_g around 40°C) supporting the conclusion.

The formation of a cross-linked network impacts also both the melting temperature and crystallinity of the material. PBT, PBT-A and to some extent the soluble fractions PBT-EZ_{sol}, and PBT-EA_{sol} exhibit a double melting endotherm (T_{m1} and T_{m2}) usually attributed to the

presence of two different distributions of lamella thickness. Upon heating, melting, recristallization, lamella thickening and crystal perfecting phenomena occur in the polymer. [**61, 62**] On the contrary, cross-linked materials display a single melting endotherm (T_{m1}) as the crystal perfection step might be prevented. Besides, PBT-EZ_{gel} and PBT-EZA_{gel} have a lower T_m compared to their partially cross-linked counterpart.

Table 3. Thermal characteristics of PBT, PBT-A, PBT-EZ, PBT-EZA and their gel and soluble part. Crystallinity of PBT-EZA_{sol} was obtained by considering the amount of FR left after solubility tests (Equation S 1 in ESI†). PBT-EZA_{gel} crystallinity could not be precisely obtained due to close proximity of the endotherm observed for AlPi (for additional details, see **Figure S1** in ESI†).

Sample	T_g (°C)	T_{m1} (°C)	T_{m2} (°C)	ΔH_m (J/g)	T_c (°C)	ΔH_c (J/g)	$\chi_{c\ PBT}$ /$\chi_{c\ PBT+FR}$ (%)
PBT	39 ± 1	215 ± 1	225 ± 2	51 ± 2	191 ± 2	51 ± 2	36 ± 1
PBT-EZ	47.1 ± 0.9	217 ± 1	/	45 ± 1	185 ± 1	46 ± 1	32 ± 1
PBT-EZ_{gel}	47.4 ± 0.6	210 ± 3	/	37 ± 1	173 ± 32	37 ± 1	26 ± 1
PBT-EZ_{sol}	40.4 ± 0.5	212 ± 1	223 ± 1	49 ± 1	190 ± 1	49.2 ± 0.9	35 ± 1
PBT-A	39.7 ± 0.7	213 ± 0.7	224 ± 1	37 ± 2	190.9 ± 0.7	42 ± 1	32 ± 2 / 26 ± 2
PBT-EZA	46 ± 1	213 ± 1	/	21 ± 2	172 ± 3	/	18 ± 2/ 16 ± 2
PBT-EZA_{gel}	46.3 ± 0.8	209 ± 1	/	/	161.7 ± 0.8	/	/
PBT-EZA_{sol}	41.1 ± 0.9	210 ± 0.7	218 ± 0.5	27.2 ± 0.6	180.0 ± 0.5	30.5 ± 0.8	29 ± 1
PBT-EA	46 ± 1	213 ± 1	/	22 ± 2	173 ± 3	/	18 ± 1 / 16 ± 1
PBT-EA_{gel}	46 ± 1	206 ± 1	/	/	164 ± 1	/	/
PBT-EA_{sol}	40 ± 1	219 ± 1	/	25 ± 1	178 ± 1	/	27 ±1

Incidentally, crystallinity evolution is on par with the decrease of T_m. A decrease of ~10% in crystallinity is observed between PBT and PBT-EZ. However, PBT-EZ_{gel} exhibits a radically lower crystallinity, with a decrease of ~30% compared to thermoplastic PBT formulations. Those results are in accordance with a previous study [**25**] related to the impact of the cross-linking ratio on PBT vitrimer crystallinity. Indeed, it was established that at higher gel fractions (>50%), cross-linking leads to a decrease of crystallinity [**25, 55**] in PBT vitrimer. Finally, the influence of the aluminum diethylphosphinate particles on the vitrimer crystallinity is clearly visible on PBT-EZA. While X_c decreases by ~10% between PBT and PBT-A, it drops by nearly 50% for PBT-EZA. This result implies that the crystallinity of the vitrimer is

much more sensitive to particle fillers compared to usual PBT thermoplastics. Even if the crystallinity of PBT-EZA$_{gel}$ could not be precisely obtained due to peak overlap, its thermograms indicate a lower value than PBT-EZA (**Figure S 1**), an evolution previously seen between PBT-EZ and PBT-EZ$_{gel}$.

3.2. Role of AlPi in the vitrimer formation

In the first part, it was shown that the incorporation of AlPi has a significant impact on the cross-linking kinetics and decreases dramatically the network relaxation times. To further understand the role of aluminum phosphinate in the synthesis of the PBT vitrimer, a sample (PEBT-A) without the Zn-based transesterification catalyst but with AlPi was synthesized. In this new sample, AlPi, which is supposed to act as a catalyst, is added at 20 wt.-% (412 mol%/[COOH+OH]), while for PBT-EZ, the Zn(II) catalyst molar ratio was 5 mol%/[COOH+OH]. **Figure 2** presents the evolution of the torque during synthesis in comparison with PBT-EZ and PBT-EZA. Even in the absence of the Zn-based transesterification catalyst, an increase in the axial force is still observed. The maximum axial force reached 5000 N around a minute later than for PBT-EZA (at 6-7 minutes), which is similar to the time observed for PBT-EZ formulation. The material presents a global gel ratio of 62wt.-% and a gel ratio without considering the FR present in the gel of 68 wt.-%. The gel ratio value of the matrix phase of the gel is similar to PBT-EZA (calculated by using **Equation 2** and **Equation 3** and data from **Table 4**). This result confirms the role of AlPi as transesterification catalyst.

Table 4. Weight percentages of Aluminum and Phosphorus remaining in PBT-EA and PBT-EA$_{gel}$ based on elemental analysis and calculated %FR and %gel

Sample	%Gel$_{PBT+FR}$	Al (wt.-%)	P (wt.-%)	%FR$_m$	%Gel$_{PBT}$
PBT-EA	62 ± 4	1.25 ± 0.02	4.28 ± 0.02	17.8	68 ± 4
PBT-EA$_{gel}$	/	0.71 ± 0.01	2.49 ± 0.01	10.4	/

The vitrimer behavior of the newly formed materials was evidenced by stress-relaxation experiments (**Figure *2*** and **Table S 3**). PBT-EA exhibits an activation energy of 179 kJ.mol^{-1}, and relaxation times that are in the same order of magnitude as PBT-EZA. Usually, transesterification-based CANs exhibit high relaxation times [**8, 25, 30-32, 63, 64**], making their synthesis hard to up-scale to a continuous process. Such low relaxation time has never been seen for any transesterification-catalyzed vitrimer, making poly(butylene terephthalate) -

aluminum phosphinate vitrimer an interesting candidate to upscale to continuous processes. Besides, PBT-EA presenting a high activation energy (E_a) compared with PBT-EZ enables to have a more sensitive temperature dependency leading to contrasted changes in viscosity. [**19**]

3.3. Impact of the vitrimer network on the FR dispersion and structure

As previously demonstrated, AlPi acts as a catalyst in the bond exchange reaction of the PBT-vitrimer network. It is consequently not an inert filler in the formulation. Thus, in this part, the impact of the formation of the vitrimer matrix on the repartition of the flame-retardant and the possible change of its chemical structure was investigated.

SEM and Microprobe analyses have first been performed on cross-sections of the extruded PBT-EA and its gel fraction PBT-EA_{gel} (**Figure 4**). Particles containing both P and Al are clearly visible in the PBT-EA sample, and can be attributed to the presence of the FR additive. Their diameters range from a few µm to up to 20 µm. These values are in the range of the particle size given by the supplier of the FR additive. On the other hand, chemical analyses were also performed on points PBT-EA-2 and PBT-EA_{gel}-1, where no particles were visible. The presence of P and Al is observed, which implies that a fraction of aluminum phosphinate has been homogeneously dispersed into the vitrimer matrix. The presence of FR in the gel fraction is also visible, however, no particles are noticeable but microprobe analysis confirmed that P and Al are homogeneously distributed in the gel or even dissolved in it. This result is to be put on par with the elemental analysis, which confirmed that around 50% of aluminum and phosphorus was still present in the gel fraction. Those results indicate that a large quantity of the AlPi is homogeneously dispersed/dissolved in the gel fraction of the vitrimer.

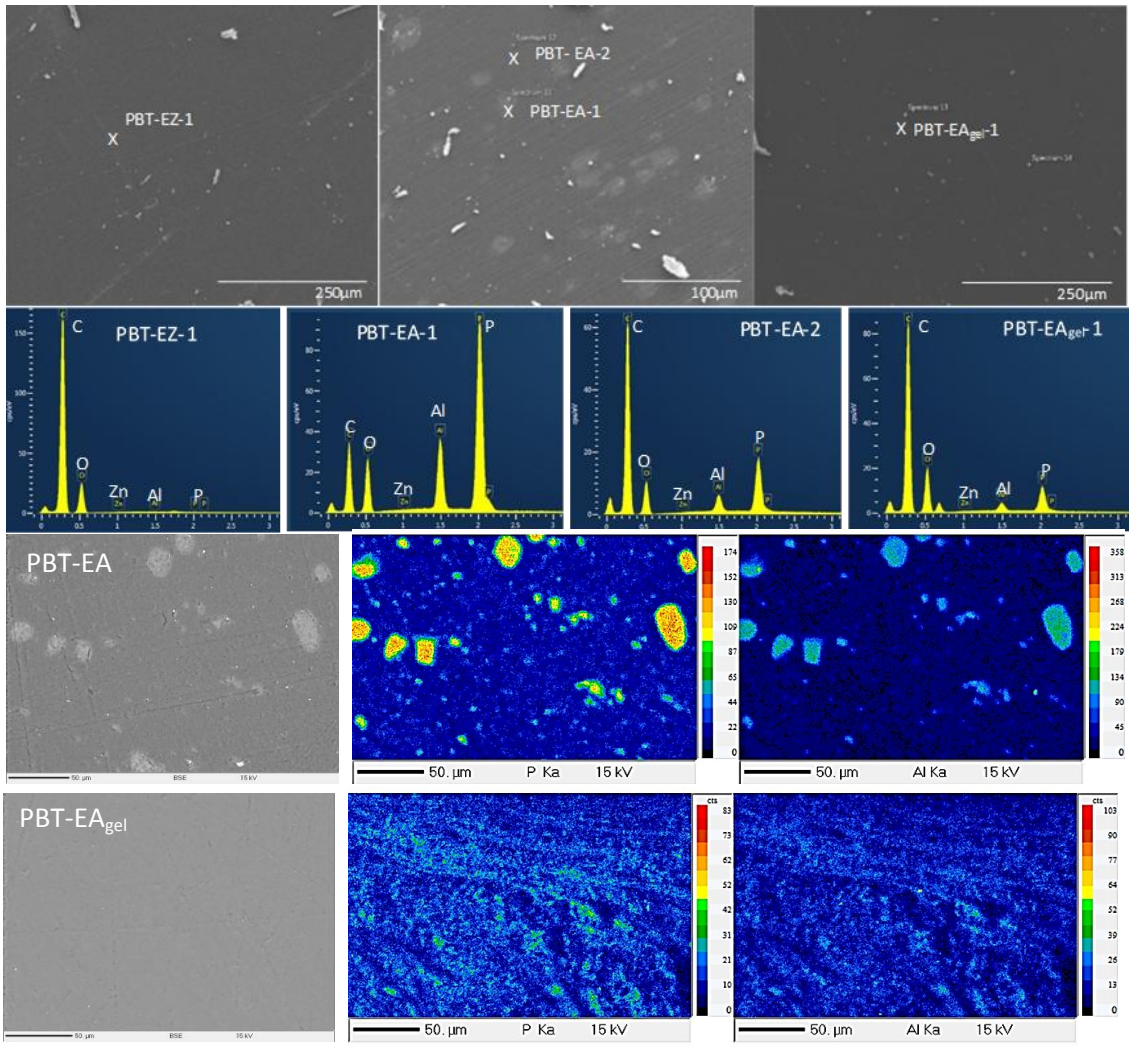

Figure 4. On top: SEM images of PBT-EZ, PBT-EA and PBT-EA$_{gel}$ and their respective EDX analysis. On the bottom: EPMA images and P and Al mappings of PBT-EA and PBT-EA$_{gel}$

To detect modification of the chemical environment around the aluminum and phosphorus atoms, ^{27}Al and ^{31}P ss NMR analyses were performed on PBT-EZA, PBT-EA and their respective gel fractions (PBT-EZA$_{gel}$ and PBT-EA$_{gel}$). The obtained spectra are represented in Figure 5. The ^{27}Al ss NMR spectrum of AlPi exhibits a single peak at -12 ppm (

Figure *5* - 1) due to the octahedral geometry of Al^{3+} cations, coordinated to phosphorus in their second coordination sphere.[**65**] On the other hand, ^{31}P ss NMR spectrum presents two peaks between 38 and 45 ppm (

Figure *5* - 2), characteristic of phosphinate sites. [**66**]

While those peaks on ^{27}Al and ^{31}P spectra are still present for PBT-EA and PBT-EZA, the analysis of their gel fraction highlights the presence of new, low-intensity signals at around 47

ppm for ^{27}Al analyses (

Figure *5* - 3), indicating either a tetracoordinated or hexacoordinated aluminum, and at 52 and 56 ppm for ^{31}P analyses (

Figure *5* - 4). These peaks could be attributed to the presence of diethylphosphinic acid [**67**]. According to the literature, this acid should exhibit a single peak round 52-53 ppm in ^{31}P NMR. It could be assumed that the presence of two peaks instead of one is due the slightly different environments surrounding the acid groups in the gel. Its presence shows that AlPi salt is partially modified. The presence of these peaks in the gel fraction could be linked to the catalytic role of AlPi in the vitrimer formation. Demongeot et al. [**59**] previously showed that Zn transesterification catalysts in vitrimers do not remain under their initial $Zn(acac)_2$ form, but undergo ligand exchanges to form active complexes structurally bonded to the network through alkoxide or carboxyl ligands. By analogy with this study, it is reasonable to assume that the Al^{3+} cation can undergo similar ligand exchanges and might also be structurally bonded to the vitrimer network. Consequently, some ligand exchanges may have occurred explaining the change in P and Al chemical environment, i.e. the "phosphinate ligands" may act as weak bases to deprotonate the β-hydroxyester, forming an alkoxide which will, in turn, either attack an ester group from the PBT backbone or serve as a ligand for Al^{3+}. The low intensity of the new peaks may be caused by the low cross-linking density of the cross-linked

network, limited by the number of reactive -COOH and -OH bonds. Thus, only low quantities of AlPi can interact with the matrix to effectively catalyze the transesterification reaction.

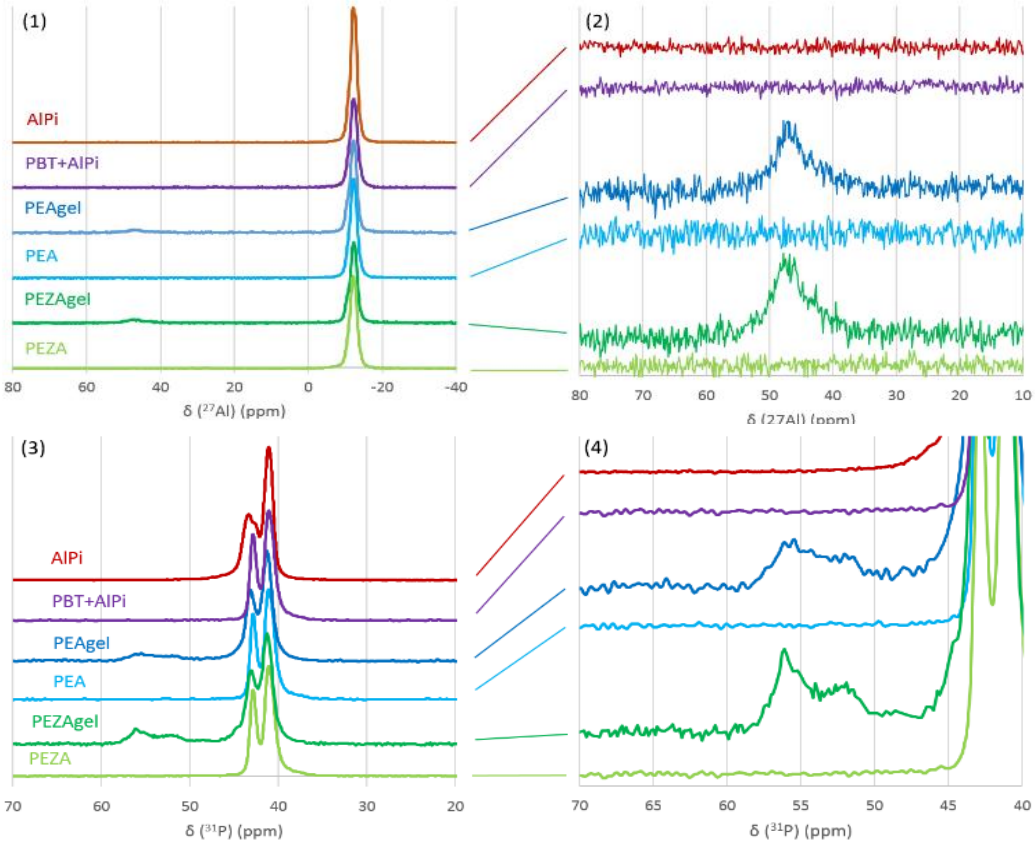

Figure 5. ^{27}Al (1) and (2) and ^{31}P solid-state NMR (3) and (4) spectra of AlPi, PBT-A, PBT-EA, PBT-EA$_{gel}$, PBT-EZA and PBT-EZA$_{gel}$; zoom on the new peak (right).

3.4. Properties of vitrimers PEA

This part aims at investigating the advantage of the vitrimer matrix on the thermal stability, fire and mechanical properties of the flame retarded PBT vitrimer material PBT-EA.

The thermal properties of the materials have first been analyzed using DSC and TGA analyses. DSC results are presented in **Table 3**. As PBT-EZ and PBT-EZA, PBT-EA and PBT-EA$_{gel}$ exhibit higher T_g of 46°C compared with their thermoplastic reference PBT-A, a single melting endotherm and similar crystallinity values on par with PBT-EZA for PBT-EA. Thus, vitrimer with AlPi as the

sole transesterification catalyst shows similar thermal properties as the vitrimer combining both AlPi and $Zn(acac)_2$.

TGA and derivative thermogravimetry (DTG) curves recorded under nitrogen for PBT, PBT-EZ, PBT-A and PBT-EA are presented in

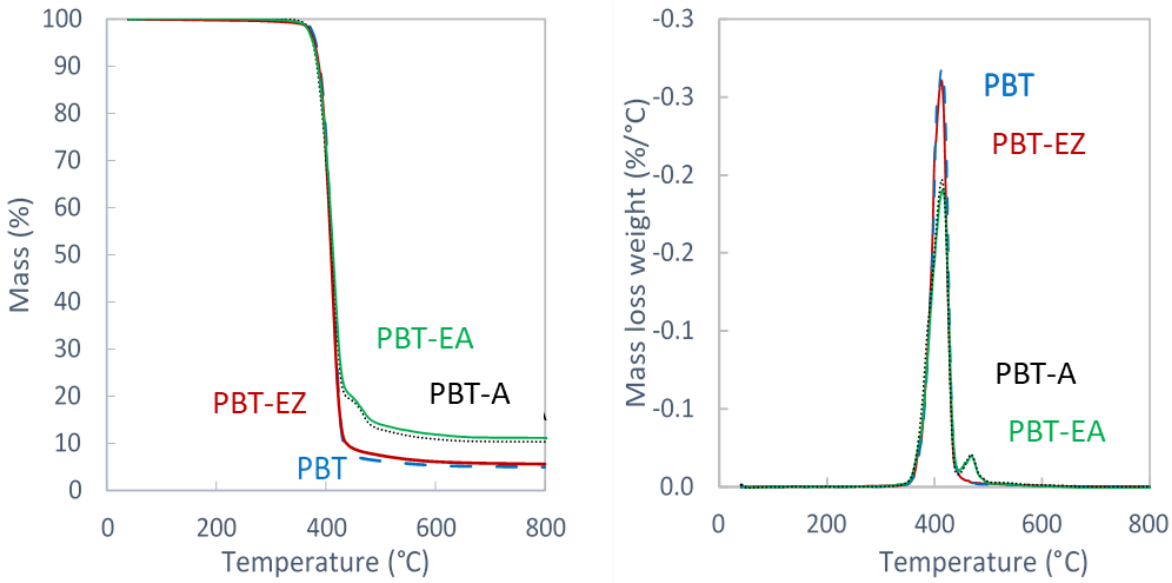

Figure 6. The materials that do not contain the flame retardant, PBT and PBT-EZ, decompose in the same way in a single step from 320 to 450°C leading to a residue of around 3 wt.-%. The flame-retarded materials present, in addition to this first step, a minor second step between 450 and 500°C. A final char residue of 12 wt.-% is found for PBT-EA and PBT-A. AlPi is known to act in the gas phase as well as in the condensed phase with the formation of a transitory residue stabilized by phosphorus that eventually decomposes at a higher temperature. [**65, 66**] As AlPi decomposes in a single step between 380 and 520°C with a residue of around 7 wt.-%, [**66**] the calculated weight of residue without interaction in the condensed phase should be around 3.8 wt.-%. Here a residue of 12 wt.-% is obtained indicating the presence of interactions in the condensed phase between PBT and AlPi decomposition products. However, the same amount of residue is obtained for the flame retarded thermoplastic and vitrimer. Whether the material is vitrimer or thermoplastic the same decomposition pathway is followed and the presence of the vitrimer network does not lead to better thermal stability.

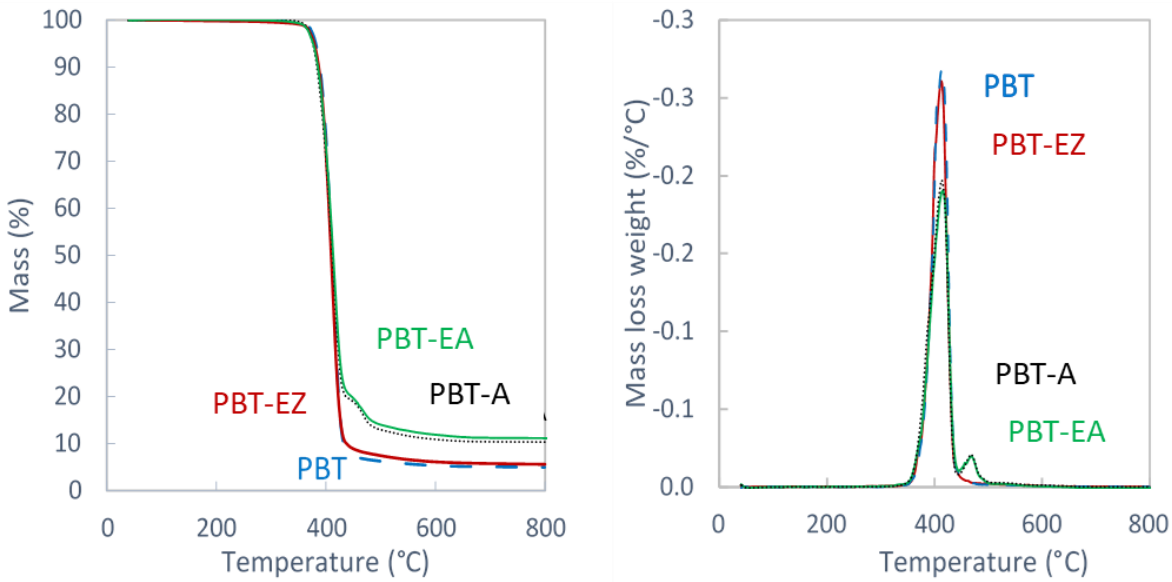

Figure 6. TGA (left) and DTG (right) of PBT (dashed), PBT-A (dashed), PBT-EZ and PBT-EA

UL-94 tests have been performed on the different materials. **Table 5** describes the classifications obtained by the different formulations as well as additional parameters measured in UL-94 tests such as the flaming time after the first and second burner exposition, the loss of flaming drops that ignite the cotton placed underneath the sample as well as the mass loss during the test.

After the first burner application, PBT exhibits a flaming time above 30 s, while flaming time for PBT-EZ does not exceed a few seconds. However, the second application of the burner leads to similar flaming times for both samples, with both materials burning intensely to the clamp after ignition with strong flaming drips inflaming the cotton. On the contrary, both 20 wt% filled materials are V0 rated, which is the best rating, with no dripping observed. A slight difference can be observed in terms of mass loss during the tests. Indeed, even if there is no dripping, part of the materials decomposes releasing gaseous degradation products that leads to a decrease of the sample mass. Here, flame- retarded vitrimer (PBT-EA) loses less mass than the flame-retarded PBT (PBT-A) (1.5 versus 3 wt.-%). Another difference can be observed in **Figure 7** between these two materials revealing the difference of melt strength. Indeed, the vitrimer samples do not elongate due to flowing at high temperatures contrary to the thermoplastics.

Overall, the aluminum phosphinate can act as a transesterification catalyst in the vitrimer system without impacting its efficiency as a flame-retardant for the matrix. It could be

interesting to further study the potential advantages of flame-retarded vitrimer by lowering the loading of flame-retardant to see if a difference in fire performance could be observed with the vitrimer matrix compared to the thermoplastic matrix and also to test different thermal constraints (cone colorimeter test or glow wire test for example).

Table 5. UL-94 classification results

Sample	$\%Gel_{PBT}$	Rating	t_1 (s)	t_2 (s)	Dripping + cotton ignition	Mass loss (wt.-%)
PBT	0	NC	>30	>30	Yes	85 ± 15
PBT-EZ	68 ± 4	NC	1 ± 1	>30	Yes	80 ± 20
PBT-A	0	V0	0	1 ± 2	No	3.0 ± 0.5
PBT-EA	69 ± 3	V0	0	1 ± 2	No	1.5 ± 0.5

NC=Not Classified, t_1 = flaming time after the first flame application; t_2 = flaming time after the second flame application

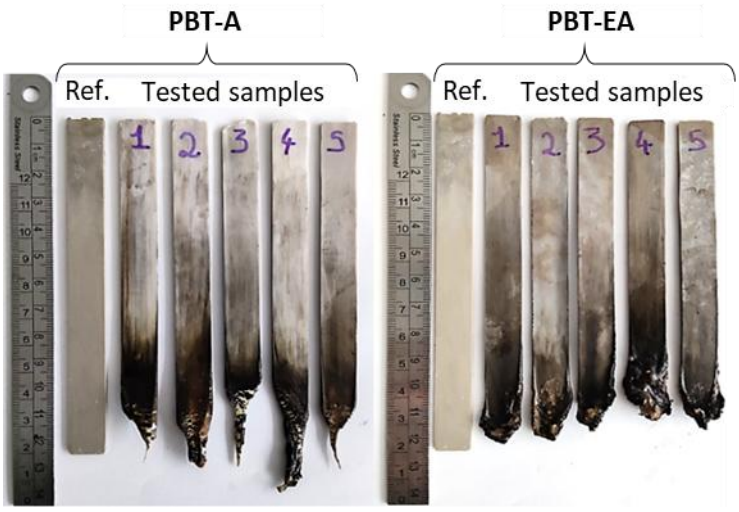

Figure 7. PBT-A and PBT-EA UL-94 samples after testing. The ruler and intact bar (ref.) are shown for illustration purpose only.

The mechanical properties of PBT, PBT-A, PBT-EZ and PBT-EA were finally evaluated in quasi-static tensile tests (**Table 6**). At room temperature, PBT exhibits a classic ductile behavior [**68**] with a yield stress of 48 MPa followed by the formation and propagation of a necking leading to a high elongation at break reaching up to 400% (**Figure 8 - 1**). Compared to virgin PBT, PBT-EZ presents an increase in the Young's modulus by 30% (1750 versus 1320 MPa), a 30% higher breaking strength (62 versus 48 MPa), a drastic decrease in the strain at break (12% versus

400%) and no necking phenomenon. This shows that the cross-linking promotes more homogeneous deformation with a strain-hardening behavior. This absence of localized plastic deformation compared with its PBT counterpart has been studied by Farge *et al.*, and was attributed to the presence of "chemical nodes" formed during cross-linking, in addition to the "physical nodes" promoted by the entanglement of the network. [**33, 34**] The crosslinked macromolecular network of the vitrimer is consequently less extensible compared to its thermoplastic counterpart leading to a lower strain at break.

When AlPi is added to the systems, Young's modulus increases by around 23% for PBT-EA compared to PBT-EZ, and 20% for PBT-A compared with PBT. However, both matrices exhibit brittle-like behavior with similar deformation at break under 4%. The incorporation of micro-sized filler is widely considered as the main factor responsible for the important changes observed in the mechanical behavior [**69, 67**]: the higher young modulus can be explained by the higher stiffness of AlPi particles compared with pristine thermoplastic or vitrimer matrices and the probable lack of adhesion between the filler and the matrix leads to the low strain at break values.

To confirm the influence of the cross-linked network on the improved stiffness, tensile tests were also conducted at 160°C i.e. far above T_g, and still below melting temperature (**Figure 8**). PBT-EA exhibits a 30% higher modulus than PBT-A while the latter exhibits a higher crystallinity than PBT-EA ($\chi_{c\ PBT+FR}$ of 26 versus 16%). This shows the impact of the cross-linked network of the vitrimer on the mechanical behavior. Moreover, PBT-EA exhibits uniform strain distribution throughout the entire specimen and is able to undergo plastic deformation without necking contrary to PBT-A (**Figure 9**). Thus, at 160°C, PBT-EA exhibits a better elongation at break (nearly double). At those temperatures, bond-exchange reactions may occur within the amorphous phase, which could promote a reconfiguration of the network inducing a homogeneous deformation.

Table 6. Mechanical properties of compound PBT, PBT-A, PBT-EZ and PBT-EA, measured by tensile testing. If not indicated, tests were conducted at room temperature.

	E (MPa)	Yield stress (MPa)	Stress at break (MPa)	Strain at break (%)
PBT	1320 ± 100	49 ± 2	48 ± 3	Up to 400
PBT-A	1600 ± 100	/	38 ± 4	4.0 ± 0.3
PBT-EZ	1750 ± 150	56 ± 3	62 ± 4	12 ± 2
PBT-EA	2150 ± 100	/	55 ± 3	3.5 ± 0.5
PBT-A (160°C)	227 ± 9	/	12 ± 1	27 ± 5

PBT-EA (160°C)	339 ± 20	/	23 ± 2	50 ± 8

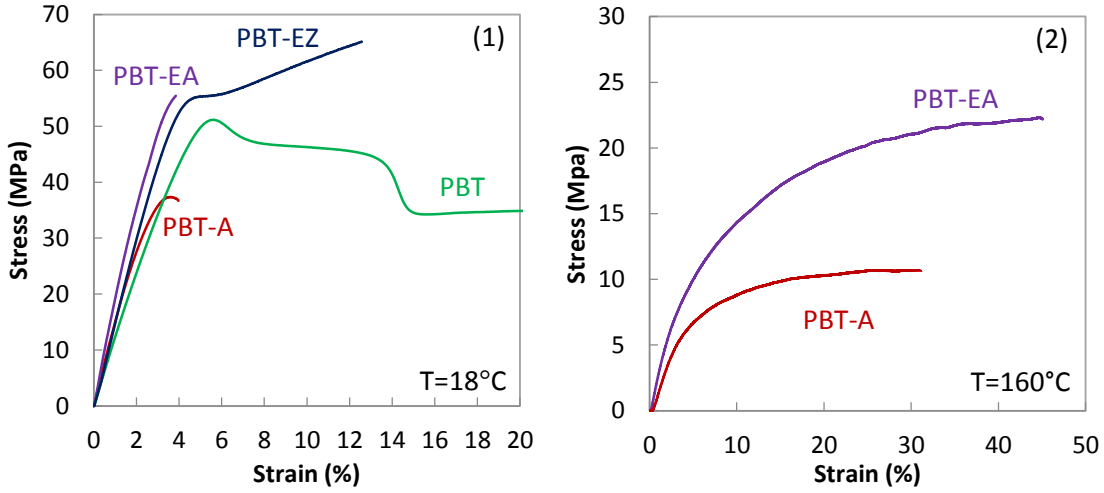

Figure 8. Stress-strain curves of the thermoplastics (PBT, PBT-A) and vitrimer equivalents (PBT-EZ, PBT-EA), at room temperature (1) and at 160°C (2).

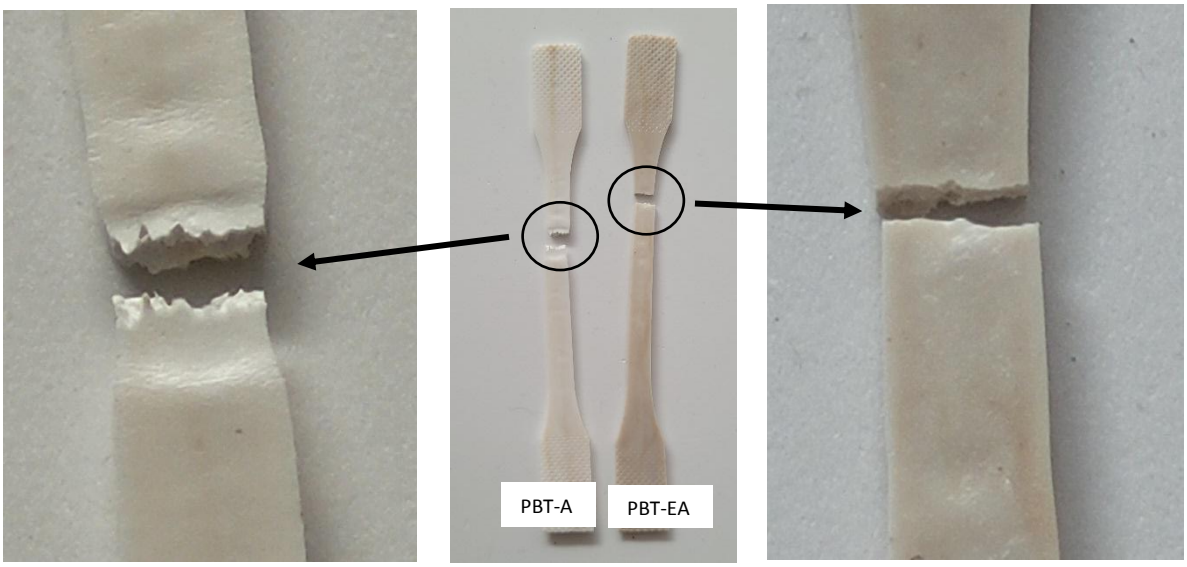

Figure 9. Pictures of dog-bone samples after tensile test at 160°C. A beginning of drawing with strain localization (necking) is visible for compound PBT-A (left), while no strain localization appears for PBT-EA (right).

IV. CONCLUSION

This paper reports the successful synthesis of fireproofed PBT-based vitrimers by reactive extrusion and using aluminum phosphinate as an FR additive. Gel content, elemental analysis, NMR studies and rheological characterizations in the melt indicate that the aluminum (III)

phosphinate salt can act as both a transesterification catalyst and an FR additive. Moreover, the fireproof PBT-based vitrimer presents better fluidity at high temperatures compared to pristine vitrimer, with a relaxation time of about a hundred times faster. This effect can be crucial considering the processing of vitrimer through reactive extrusion. The thermal analysis highlights a steep decrease in crystallinity for filled vitrimers compared to PA, a T_g similar to PBT vitrimer without fire retardant. Interestingly, the filled vitrimer presents better mechanical performances than PA, with a higher tensile strength while keeping similar thermal degradation behavior.

The existence of several types of commercially available flame-retardant salts constitutes a great opportunity to create a potential easy-to-design flame-retarded PBT-vitrimer with unique fluidity. Besides, as PBT-aluminum phosphinate vitrimers seem to show better dimensional stability during fire than thermoplastic PBT-AlPi, ongoing research is dedicated to obtain PBT vitrimers with similar thermal properties while reducing the amount of phosphinate required.

Acknowledgements:

The Chevreul Institute is thanked for its help in the development of this work through the ARCHI-CM project supported by the "Ministère de l'Enseignement Supérieur de la Recherche et de l'Innovation", the region "Hauts-de-France", the European Regional Development Fund (ERDF) program of the European Union and the "Métropole Européenne de Lille". The authors would like to thank Mr. Bertrand Revel for its help in carrying out the work on the solid state NMR facility of the Advanced Characterization Platform of the Chevreul Institute. This work was supported by the Univeristy of Lille and the region "Hauts de France".

Funding: This work was supported by the University of Lille and the region "Hauts de France".

Data Availability Statement: The data presented in this study are available on request from the corresponding author.

Author contributions: Louis Meunier: Investigation, Writing - Original Draft, Visualization, Conceptualization, Methodology. **Fabienne Samyn**: Funding acquisition, Conceptualization, Validation, Visualization, Project administration, Supervision, Methodology, Writing - Review & Editing. **Sophie Duquesne**: Project administration, Validation, Methodology, Writing - Review & Editing. **Valérie Gaucher**: Validation, Writing - Review & Editing. **David Fournier**: Writing - Review & Editing. **Damien Montarnal**: Visualization, Writing - Review & Editing. All authors have read and agreed to the published version of the manuscript.

Conflicts of Interest: The authors declare no conflict of interest. The funders had no role in the design of the study; in the collection, analyses, or interpretation of data; in the writing of the manuscript, or in the decision to publish the results.

References:

1. Rowles, W. Celanex thermoplastic polyester (PBT) — properties, design and processing. *Materials & Design* **7**, 89–94 (1986).
2. Miller, S. Macrocyclic polymers from cyclic oligomers of poly(butylene terephthalate). *Doctoral Dissertations Available from Proquest* 1–253 (1998).
3. Casu, A. *et al.* Effect of glass fibres and fire retardant on the combustion behaviour of composites, glass fibres–poly(butylene terephthalate). *Fire and Materials* **22**, 7–14 (1998).
4. Vu-Khanh, T., Denault, J., Habib, P. & Low, A. The effects of injection molding on the mechanical behavior of long-fiber reinforced PBT/PET blends. *Composites Science and Technology* **40**, 423–435 (1991).
5. Tjahjadi, M. & Gallucci, R. R. Tracking resistance of flame retardant glass reinforced PBT. in vol. 2 1168–1172 (1998).
6. Mohd Ishak, Z. A., Leong, Y. W., Steeg, M. & Karger-Kocsis, J. Mechanical properties of woven glass fabric reinforced in situ polymerized poly(butylene terephthalate) composites. *Composites Science and Technology* **67**, 390–398 (2007).

7. Köppl, T. *et al.* Structure−property relationships of halogen-free flame-retarded poly(butylene terephthalate) and glass fiber reinforced PBT. *Journal of Applied Polymer Science* **124**, 9–18 (2012).

8. Montarnal, D., Capelot, M., Tournilhac, F. & Leibler, L. Silica-Like Malleable Materials from Permanent Organic Networks. *Science* **334**, 965–968 (2011).

9. Zheng, J., Png, Z.M., Ng, S.H., Tham, G.X., Ye, E., Goh, S.S., Loh, X.J., Li, Z. Vitrimers: Current research trends and their emerging applications. *Materials Today* **51**, 586- 625 (2021).

10. Taynton, P. *et al.* Heat- or Water-Driven Malleability in a Highly Recyclable Covalent Network Polymer. *Advanced Materials* **26**, 3938–3942 (2014).

11. Geng, H. *et al.* Vanillin-Based Polyschiff Vitrimers: Reprocessability and Chemical Recyclability. *ACS Sustainable Chem. Eng.* **6**, 15463–15470 (2018).

12. Lu, Y.-X. & Guan, Z. Olefin metathesis for effective polymer healing via dynamic exchange of strong carbon-carbon double bonds. *Journal of the American Chemical Society* **134**, 14226–14231 (2012).

13. Lu, Y.-X., Tournilhac, F., Leibler, L. & Guan, Z. Making Insoluble Polymer Networks Malleable via Olefin Metathesis. *J. Am. Chem. Soc.* **134**, 8424–8427 (2012).

14. Röttger, M. *et al.* High-performance vitrimers from commodity thermoplastics through dioxaborolane metathesis. *Science* **356**, 62–65 (2017).

15. Cromwell, O. R., Chung, J. & Guan, Z. Malleable and Self-Healing Covalent Polymer Networks through Tunable Dynamic Boronic Ester Bonds. *J. Am. Chem. Soc.* **137**, 6492–6495 (2015).

16. Hendriks, B., Waelkens, J., Winne, J. M. & Du Prez, F. E. Poly(thioether) Vitrimers via Transalkylation of Trialkylsulfonium Salts. *ACS Macro Letters* **6**, 930–934 (2017).

17. Majumdar, S. *et al.* Phosphate Triester Dynamic Covalent Networks. *ACS Macro Letters* **9**, 1753–1758 (2020).

18. Denissen, W. *et al.* Vinylogous Urethane Vitrimers. *Adv. Funct. Mater.* **25**, 2451–2457 (2015).

19. Denissen, W. *et al.* Chemical control of the viscoelastic properties of vinylogous urethane vitrimers. *Nature Communications* **8**, (2017).

20. Denissen, W. *et al.* Vinylogous Urea Vitrimers and Their Application in Fiber Reinforced Composites. *Macromolecules* **51**, 2054–2064 (2018).

21. Lessard, J. J. *et al.* Catalyst-Free Vitrimers from Vinyl Polymers. *Macromolecules* **52**, 2105–2111 (2019).

22. Tellers, J., Pinalli, R., Soliman, M., Vachon, J. & Dalcanale, E. Reprocessable vinylogous urethane cross-linked polyethylene via reactive extrusion. *Polym. Chem.* **10**, 5534–5542 (2019).

23. Wright, T., Tomkovic, T., Hatzikiriakos, S. G. & Wolf, M. O. Photoactivated Healable Vitrimeric Copolymers. *Macromolecules* **52**, 36–42 (2019).

24. Bai, L. & Zheng, J. Robust, reprocessable and shape-memory vinylogous urethane vitrimer composites enhanced by sacrificial and self-catalysis Zn(II)–ligand bonds. *Composites Science and Technology* **190**, 108062 (2020).

25. Demongeot, A. *et al.* Cross-Linking of Poly(butylene terephthalate) by Reactive Extrusion Using Zn(II) Epoxy-Vitrimer Chemistry. *Macromolecules* **50**, 6117–6127 (2017).

26. Caffy, F. & Nicolaÿ, R. Transformation of polyethylene into a vitrimer by nitroxide radical coupling of a bis-dioxaborolane. *Polymer Chemistry* **10**, 3107–3115 (2019).

27. Breuillac, A., Caffy, F., Vialon, T. & Nicolaÿ, R. Functionalization of polyisoprene and polystyrene: Via reactive processing using azidoformate grafting agents, and its application to the synthesis of dioxaborolane-based polyisoprene vitrimers. *Polymer Chemistry* **11**, 6479–6491 (2020).

28. Taplan, C., Guerre, M., Winne, J. M. & Du Prez, F. E. Fast processing of highly crosslinked, low-viscosity vitrimers. *Materials Horizons* **7**, 104–110 (2020).

29. Maaz, M., Riba-Bremerch, A., Guibert, C., Van Zee, N. J. & Nicolaÿ, R. Synthesis of Polyethylene Vitrimers in a Single Step: Consequences of Graft Structure, Reactive Extrusion Conditions, and Processing Aids. *Macromolecules* **54**, 2213–2225 (2021).

30. Zhou, Y., Goossens, J. G. P., Sijbesma, R. P. & Heuts, J. P. A. Poly(butylene terephthalate)/Glycerol-based Vitrimers via Solid-State Polymerization. *Macromolecules* **50**, 6742–6751 (2017).

31. Zhou, Y., Goossens, J. G. P., van den Bergen, S., Sijbesma, R. P. & Heuts, J. P. A. In Situ Network Formation in PBT Vitrimers via Processing-Induced Deprotection Chemistry. *Macromolecular Rapid Communications* **39**, (2018).

32. Zhou, Y., Groote, R., Goossens, J. G. P., Sijbesma, R. P. & Heuts, J. P. A. Tuning PBT vitrimer properties by controlling the dynamics of the adaptable network. *Polymer Chemistry* **10**, 136–144 (2019).

33. Farge, L., Hoppe, S., Daujat, V., Tournilhac, F. & Andre, S. Solid Rheological Properties of PBT-Based Vitrimers. *Macromolecules* **54**, 1838–1849 (2021).

34. Farge, L. *et al.* Development of plasticity in vitrimers synthesized from a semi-crystalline polymer using injection molding. *Journal of Polymer Science* **60**, 1962–1975 (2022).

35. Zhou, L. *et al.* Design of a self-healing and flame-retardant cyclotriphosphazene-based epoxy vitrimer. *J Mater Sci* **53**, 7030–7047 (2018).

36. Markwart, J. C. *et al.* Intrinsic flame retardant phosphonate-based vitrimers as a recyclable alternative for commodity polymers in composite materials. *Polym. Chem.* **11**, 4933–4941 (2020).

37. Feng, X. & Li, G. Versatile Phosphate Diester-Based Flame Retardant Vitrimers via Catalyst-Free Mixed Transesterification. *ACS Applied Materials and Interfaces* **12**, 57486–57496 (2020).

38. Feng, X. & Li, G. Catalyst-free β-hydroxy phosphate ester exchange for robust fire-proof vitrimers. *Chemical Engineering Journal* **417**, (2021).

39. Aufmuth, W., Levchik, S. v., Levchik, G. f. & Klatt, M. Poly(butylene terephthalate) fire retarded by 1,4-diisobutylene-2,3,5,6-tetraxydroxy-1, 4-diphosphine oxide. I. Combustion and thermal decomposition. *Fire and Materials* **23**, 1–6 (1999).

40. Levchik, S. V. & Weil, E. D. Flame retardancy of thermoplastic polyesters—a review of the recent literature. *Polymer International* **54**, 11–35 (2005).

41. Klatt, M. D., Gareis, B. D. & Yamamoto, M. . Flame proofed moulding materials. EP0932642B1 (April 23, 1998).

42. Levchik, S. V., Bright, D. A., Alessio, G. R. & Dashevsky, S. Synergistic action between aryl phosphates and phenolic resin in PBT. *Polymer Degradation and Stability* **77**, 267–272 (2002).

43. Klatt, M., Heitz, T. & Gareiss, B. Flame-proof thermoplastic moulding materials. US6306941B1 (October 23, 2001).

44. Van, D. S. P. a, Bos, M. L. M., Roovers, W. a C., Van, G. M. & Menting, H. N. a M. Halogen-free flame-retardant composition. US6767941B2 (July 27, 2004).

45. Balabanovich, A. I., Levchik, G. F., Levchiky, S. V. & Engelmann, J. Fire Retardant Synergism Between Cyclic Diphosphonate Ester and Melamine in Poly(Butylene Terephthalate). *Journal of Fire Sciences* **20**, 71–83 (2002).

46. Jenewein, E., Kleiner, H.-J., Wanzke, W. & Budzinsky, W. Synergistic flame protection agent combination for thermoplastic polymers. (2002).

47. Gallo, E., Braun, U., Schartel, B., Russo, P. & Acierno, D. Halogen-free flame retarded poly(butylene terephthalate) (PBT) using metal oxides/PBT nanocomposites in combination with aluminium phosphinate. *Polymer Degradation and Stability* **94**, 1245–1253 (2009).

48. Braun, U., Bahr, H., Sturm, H. & Schartel, B. Flame retardancy mechanisms of metal phosphinates and metal phosphinates in combination with melamine cyanurate in glass-fiber reinforced poly(1,4-butylene terephthalate): the influence of metal cation. *Polymers for Advanced Technologies* **19**, 680–692 (2008).

49. Levchik, G. F., Grigoriev, Y. V., Balabanovich, A. I., Levchik, S. V. & Klatt, M. Phosphorus–nitrogen containing fire retardants for poly(butylene terephthalate). *Polymer International* **49**, 1095–1100 (2000).

50. Legrand, A. & Soulié-Ziakovic, C. Silica-Epoxy Vitrimer Nanocomposites. *Macromolecules* **49**, 5893–5902 (2016).

51. Yang, Z., Wang, Q. & Wang, T. Dual-Triggered and Thermally Reconfigurable Shape Memory Graphene-Vitrimer Composites. *ACS Appl. Mater. Interfaces* **8**, 21691–21699 (2016).

52. Poutrel, Q.-A., Baghdadi, Y., Souvignet, A. & Gresil, M. Graphene functionalisations: Conserving vitrimer properties towards nanoparticles recovery using mild dissolution. *Composites Science and Technology* **216**, 109072 (2021).

53. Yue, L., Amirkhosravi, M., Ke, K., Gray, T. G. & Manas-Zloczower, I. Cellulose Nanocrystals: Accelerator and Reinforcing Filler for Epoxy Vitrimerization. *ACS Appl. Mater. Interfaces* **13**, 3419–3425 (2021).

54. Yang, Y. *et al.* Carbon nanotube-vitrimer composite for facile and efficient photo-welding of epoxy. *Chemical Science* **5**, 3486–3492 (2014).

55. Panagiotopoulos, C., Porfyris, A., Korres, D. & Vouyiouka, S. Solid-state polymerization as a vitrimerization tool starting from available thermoplastics: The effect of reaction temperature. *Materials* **14**, 1–18 (2021).

56. Pyda, M., Nowak-Pyda, E., Mays, J., & Wunderlich, B. Heat capacity of poly (butylene terephthalate). *Journal of Polymer Science Part B: Polymer Physics* **42**(23), 4401-4411 (2004).

57. Joosten L.M.A., Cassagnau P., Drockenmuller E., Montarnal D. Synthesis, Recycling and High-Throughput Reprocessing of Phase-Separated Vitrimer-Thermoplastic Blends. Advanced Functional Materials. 2306882 (2023)

58. Li, L., Chen, X., Jin, K. & Torkelson, J. M. Vitrimers Designed Both To Strongly Suppress Creep and To Recover Original Cross-Link Density after Reprocessing: Quantitative Theory and Experiments. *Macromolecules* **51**, 5537–5546 (2018).

59. Guggari, S. *et al.* Vanillin-Based Epoxy Vitrimers: Looking at the Cystamine Hardener from a Different Perspective. *ACS Sustainable Chem. Eng.* **11**, 6021–6031 (2023).

60. Demongeot, A., Mougnier, S. J., Okada, S., Soulié-Ziakovic, C. & Tournilhac, F. Coordination and catalysis of Zn^{2+} in epoxy-based vitrimers. *Polym. Chem.* **7**, 4486–4493 (2016).

61. Nichols, M. E. & Robertson, R. E. The origin of multiple melting endotherms in the thermal analysis of polymers. *Journal of Polymer Science Part B: Polymer Physics* **30**, 305–307 (1992).

62. Yeh, J. T. & Runt, J. Multiple melting in annealed poly(butlene terephthalate). *Journal of Polymer Science Part B: Polymer Physics* **27**, 1543–1550 (1989).

63. Niu, X. *et al.* Dual Cross-linked Vinyl Vitrimer with Efficient Self-Catalysis Achieving Triple-Shape-Memory Properties. *Macromolecular Rapid Communications* **40**, (2019).

64. Kar, G. P., Saed, M. O. & Terentjev, E. M. Scalable upcycling of thermoplastic polyolefins into vitrimers through transesterification. *J. Mater. Chem. A* **8**, 24137–24147 (2020).

65. Duquesne, S. *et al.* Study of the thermal degradation of an aluminium phosphinate–aluminium trihydrate combination. *Thermochimica Acta* **551**, 175–183 (2013).

66. Samyn, F. & Bourbigot, S. Thermal decomposition of flame retarded formulations PA6/aluminum phosphinate/melamine polyphosphate/organomodified clay: Interactions between the constituents? *Polymer Degradation and Stability* **97**, 2217–2230 (2012).

67. Liu, Z., Wang, J., Zhu, J., Jiao, D., Xie, Z.,Zhong, L. Diethyl phosphinate fire retardation agent preparation method, CN103319524 (A) — 2013-09-25

68. Sperling, L.H., Mechanical Behavior of Polymers. in *Introduction to Physical Polymer Science* 557–612 (John Wiley & Sons, Ltd, 2005). doi:10.1002/0471757128.ch11.

69. Botan, M., Georgescu, C. & Deleanu, L. Influence of Micro Glass Beads Added in a PBT Matrix on the Mechanical Properties of Composites. *The Annals of "Dunarea de Jos" University of Galati. Fascicle IX, Metallurgy and Materials Science* **35**, 64–71 (2012).